Journal of Materials Chemistry C

Accepted Manuscript

This article can be cited before page numbers have been issued, to do this please use: X. Zhu, H. Huang, R. Liu, X. Jin, Y. Li, D. Wang, Q. Wang and H. Zhu, *J. Mater. Chem. C*, 2015, DOI: 10.1039/C4TC02955K.

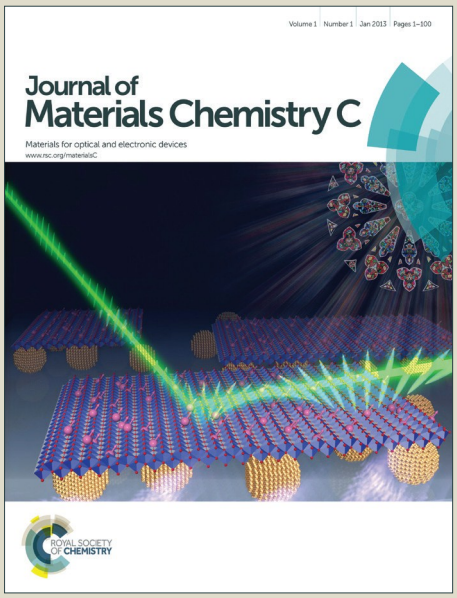

ROYAL SOCIETY OF CHEMISTRY

www.rsc.org/materialsC

Journal of Materials Chemistry C

Dynamic Article Links ►
View Article Online
DOI: 10.1039/C4TC02955K

Cite this: DOI: 10.1039/c0xx00000x

www.rsc.org/Materials C

ARTICLE TYPE

Aza-boron-diquinomethene complexes bearing *N*-aryl chromophores: synthesis, crystal structures, tunable photophysics, protonation effect and their application for pH sensor

Xiaolin Zhu,[a] Hai Huang,[a] Rui Liu,*[a] Xiaodong Jin,[a] Yuhao Li,[b] Danfeng Wang,[a] Qiang Wang,[a] Hongjun Zhu*[a]

Received (in XXX, XXX) Xth XXXXXXXXX 20XX, Accepted Xth XXXXXXXXX 20XX
DOI: 10.1039/b000000x

A series of aza-boron-diquinomethene complexes (**1a**-**1e**) bearing different *N*-aryl chromophores were synthesized and characterized by multinuclear NMR spectroscopy, X-ray crystallography, optical absorption and emission spectroscopy, and elemental analysis. These robust thermal complexes possess tunable intense luminescence from blue to red with relatively high emission quantum yields. The introduction of different *N*-aryl chromophores to the aza-BODIQU core significantly tuned the emission colors. The relationship between structure and property was investigated systematically *via* spectroscopic methods and simulated by density functional theory (DFT) calculations. Additionally, the application of **1c** for pH sensor with remarkable colour-changing property has been investigated. All these results indicate that these complexes exhibit the robust thermal stability, tunable photophysical properties, relatively high photoluminescence quantum yields and protonation effect, making these complexes potential candidates in pH sensor, bioimaging probe and organic light-emitting materials.

Introduction

Research on boron dipyrromethene (BODIPY) complexes have attracted a great deal of attention in the past decade, due to their broad applications in molecular probes,[1] photodynamic therapy,[2] laser dyes,[3] nonlinear optics,[4] and dye-sensitized solar cells,[5] *etc.*[6] The versatile applications of BODIPYs are intrinsically based on their narrow absorption and emission bands, large molar absorption coefficients, high fluorescence quantum yields and outstanding chemical stability. Recently, structural modification of BODIPYs for fine-tuning of their optical and physical properties has been extensively explored in energy conversion devices (organic light-emitting devices, OLEDs, and organic photovoltaics, OPV),[7] solar energy conversion,[8] and NIR-absorbing systems.[9] To meet the different requirements for diverse applications, considerable work has been carried out on tailoring of BODIPY cores, such as converting the traditional boron dipyrromethene to boron dipyrroamine, boron diindolamine, boron dipyridoamine, and boron diquinolinamine, *ect*.[1-9] Among them, diquinolinamine derivatives have been the subject of significant study by virtue of their structure stability, good electron-transport properties and high glass-transition temperatures.[10, 11]

During our previous work, we reported a series of aza-boron-diquinomethene (aza-BODIQU) complexes with different aryl-substituents that can be used as efficient organic light-emitting materials.[12] All these complexes exhibit robust thermal stability, intense blue to green emission and relatively high photoluminescence quantum yields. Moreover, their low-lying LUMO (lowest unoccupied molecular orbital) energy levels (~ -2.63 to -2.92 eV), are desirable for electron transfer. In addition, we also reported an aza-BODIQU complex bearing *N*-substituted phenothiazine chromophores as multi-stimuli-responsive luminescent material, which can be utilized in data encryption and decryption based on the protonation-deprotonation effect.[13] It has been clearly demonstrated that diquinolinamine could be an excellent building block in the construction of aza-BODIQU based functional luminescent materials.

Although the previous work is intriguing, the investigation on the aza-BODIQUs based luminescent materials is still limited. Furthermore, most of the reported aza-BODIQU complexes only exhibit luminescence in the region of blue-green. Clearly, aza-BODIQU based luminescent materials with a tunable emission region are desirable, challengeable and potentially valuable. We also seek to improve their luminescent properties by structural modification. To this end, we choose an alternative strategy for developing a series of new aza-BODIQU complexes by introducing electron-donating chromophors on the aza-BODIQU core directly. We envision that by incorporating *N*-aryl chromophors (*N*-arylaminos) with different electron-donating

View Article Online
DOI: 10.1039/C4TC02955K

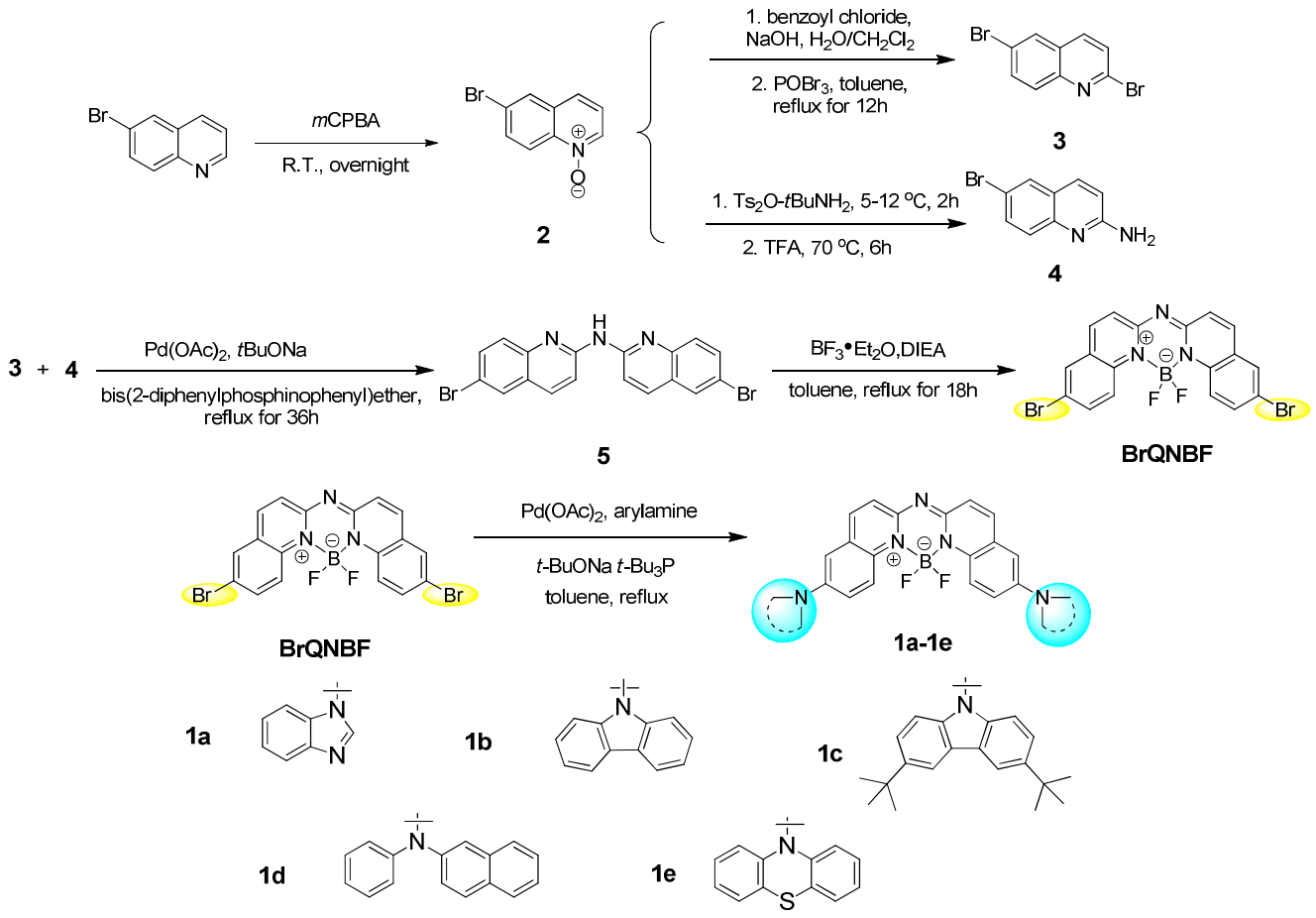

Scheme 1. Synthetic routes of complexes **1a**-**1e**.

ability and shortening the π-conjugation length between aza-BODIQU core and peripheral chromophores, the HOMO (highest occupied molecular orbital)/LUMO energies of these complexes will be significantly tuned, hence, their emission region could be extended accordingly. We also anticipate that the ground-state absorption and fluorescence quantum yield of the new complexes could be enhanced.

In this work, a series of aza-BODIQU complexes (**1a**-**1e**) with different arylamino-substituents, structurally, *N*-benzoimidazolyl, *N*-carbazolyl, 3,6-di-*tert*-butyl-*N*-carbazolyl, *N*-naphthalen-2-yl(phenyl)amino and *N*-phenothiazinyl groups were synthesized (Scheme 1). Compared to the previous aza-BODIQU complexes which mainly show blue-green emission, the emission colors of these complexes (**1a**-**1e**) are ranging from blue to red. The photophysical, crystal structures and electrochemical properties of complexes **1a**-**1e** were investigated systematically. Additionally, fluorescence of **1c** changes based on protonation effect have been investigated, which show that different acidic/basic atmospheres can induce a switch in the emission from green to red.

Results and discussion

Synthesis and characterization

Scheme 1 illustrates the synthesis of aza-BODIQU complexes (**1a**-**1e**). The Buchwald-Hartwig coupling reactions yielded the desired final products in 21-73% yields. All the products are air-stable and soluble in CH_2Cl_2, ethylacetate (EA), tetrahydrofuran (THF), dimethylformamide (DMF) and dimethyl sulphoxide (DMSO) in varying degrees. ^{1}H NMR, ^{13}C NMR, ^{19}F NMR and elemental analyses confirmed the proposed structures for all complexes except **1a**. ^{13}C NMR data of **1a** was not obtained due to its poor solubility, although different solvents were attempted.

X-ray crystallography

Single crystals of compound **1b, 1c** and **1e** suitable for X-ray analysis were successfully obtained and their crystal structures were determined. Disappointingly, efforts to grow good-quality crystals of compounds **1a** and **1d** were unsuccessful. The molecular structures of compound **1b, 1c** and **1e** are shown in Fig. 1. **1b**, **1c** and **1e** crystallize in the triclinic *P-1*, monoclinic *P2$_1$/c*, and triclinic *P-1* space groups, respectively. Their bond lengths and angles are within the typical range. The details of the crystallographic data for these crystals are summarized in Table S4 (ESI†).

As anticipated, all these complexes adopt twisted conformations. In complex **1b**, the two *N*-carbazole rings are twisted out of the planar core structure, with dihedral angles of

View Article Online
DOI: 10.1039/C4TC02955K

63.4° and 67.1°, respectively. For complex **1c**, the 3,6-di-*tert*-butyl-*N*-carbazole rings form dihedral angles of 55.9° and 40.6° with the aza-BODIQU core. Whereas for **1e**, in which the two *N*-aryl chromophores are *N*-phenothiazine rings, the bowl-shaped phenothiazine rings are almost vertically twisted from the planar aza-BODIQU core (Fig. 1). This quite obvious intramolecular torsion indicates that such a noncoplanar structure will prevent the molecules from packing in a close π-π stacking mode, which are proven by their packing motifs in packing diagrams (Fig. S15-17, ESI†). Strong intermolecular *π*-*π* interactions and other strong intermolecular interactions are almost absent. At the same time, the intramolecular bond rotational and vibrational freedom is still restricted by the intermolecular C-H…π hydrogen bonds formed between the aromatic hydrogen and the aromatic rings. And one **1b** molecule forms two C-H…F hydrogen bonds with two of its neighbor molecules (Fig. S15, ESI†). The distances of the intramolecular C-H…F hydrogen bonds range from 2.38 Å to 2.52 Å. The weak interactions between two neighbor molecules are from 3.73 to 3.79 Å. Similarly, complex **1c** molecule forms two C-H…F hydrogen bonds with its two neighbor molecules. The distances of the intramolecular C-H…F hydrogen bonds range from 2.30 Å to 2.54 Å. The weak interactions between two neighbor molecules are from 3.71 to 3.73 Å (Fig. S16, ESI†). Whereas for **1e**, the complexes adopt a stacking mode of H-type aggregation along *a* axis *via* intermolecular C-H···F, *π*-*π* and C-H···π interaction, and the vertical distance between them was measured to be 3.51 Å (Fig. S17, ESI†). These weak intermolecular interactions plus the twisted intramolecular geometries are the factors that account for the strong fluorescence of **1b**, **1c** and **1e** in the solid state.

Table 1. Thermal properties of aza-BODIQUs **1a**-**1e** [a].

Complex	T_m (°C)
1a	266
1b	383
1c	250
1d	283
1e	315

[a] DSC scans of **1a**-**1e** recorded under nitrogen during the second heating cycle at a scan rate of 10 °C min^{-1}.

Thermal properties

The thermal properties of compounds **1a**-**1e** were investigated by differential scanning calorimetry (DSC) analyses, the results are listed in Table 1. These complexes are thermally stable and lack any detectable phase transitions from 50 °C to 230 °C. Furthermore, all these complexes exhibit endothermic peaks, good thermal stability with high melt transitions temperatures (> 250 °C), which indicate excellent thermal stability and are suitable for the application of optical devices, such as the OLEDs.

Electronic absorption

The UV-Vis absorption of aza-BODIQUs (**1a**-**1e**) obeys Lambert-Beer's law in the concentration range studied (1×10^{-6} - 1×10^{-4} mol L^{-1}) in CH_2Cl_2, suggesting that no dimerization or oligomerization occurs within this concentration range in CH_2Cl_2 . The UV-Vis absorption spectra of **1a**-**1e** in CH_2Cl_2 and solid state are presented in Fig. 2. The photophysical parameters are listed in Table 2. As shown in Fig. 2a and Table 2, complex **1a** shows sharp and strong absorption (ε = 1.65 × 10^5 L mol^{-1} cm^{-1}) in the range of 391-443 nm, which is ascribed to the $^1\pi$-π^* transitions localized on the conjugated aromatic rings, considering its intense and structured absorption bands and minor solvatochromic effect (Fig. S18, ESI†). In the other hand,

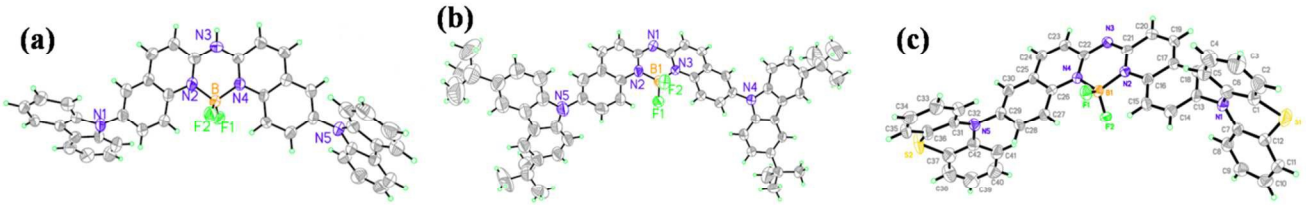

Fig. 1. Molecular structures of **1b** (CCDC 885792), **1c** (CCDC 1021584) and **1e** (CCDC 996071) obtained by X-ray diffraction.

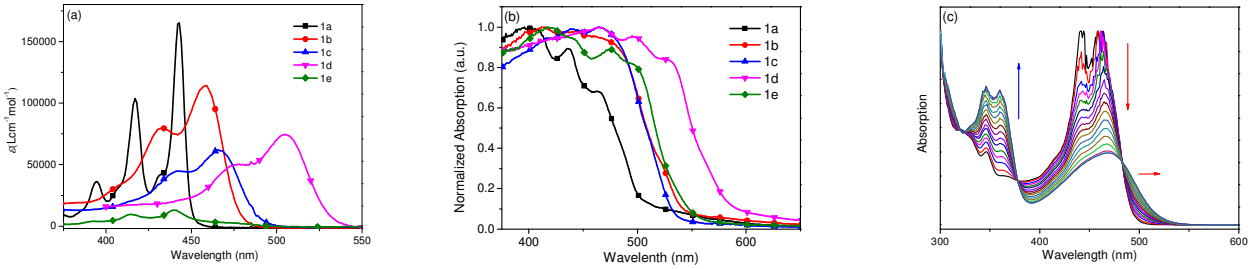

Fig. 2. (**a**) UV-Vis absorption spectra of **1a**-**1e** in CH_2Cl_2 (1×10^{-5} M); (**b**) UV-Vis absorption spectra of **1a**-**1e** in solid state; (**c**) UV/Vis spectra of **1c** in CH_2Cl_2 with addition of *p*-TsOH /CH_3CN solution.

View Article Online
DOI: 10.1039/C4TC02955K

complexes **1b**-**1e** show relatively broad bands (ε = 1.4 × 10^4 - 1.1 × 10^5 L mol^{-1} cm^{-1}) in the range of 438-505 nm, which can be ascribed to the $^1\pi$-π* mixed intramolecular charge transfer (^{1}ICT) transitions. The solvent effect also supports the nature of $^1\pi$-π* mixed ^{1}ICT transitions for their absorption bands (Fig. S18, ESI†). The possible mixture of the ^{1}ICT character could be ascribe to the strong electron-donating *N*-Aryl chromophors. It is further supported by the acid titration study with *p*-TsOH, which shows red-shifted ^{1}ICT for **1b**-**1d** in acidic solution (Fig. S23, ESI†). As shown in Fig. 2c, for **1c**, upon addition of *p*-TsOH, the absorption band at about 466 nm decreases with peak red-shift, accompanied by the increase of a new absorption band at about 337 nm. A similar phenomenon was observed for **1b** and **1d**. In addition, compared with the absorption spectra in solution, broader absorption bands with significant bathochromic shifts are observed in the solid state (Fig. 2b and Table 2). This could be attributed to the molecular stacking in the solid state, which suggests an increased π-conjugation length in their solid state due to the π-stacking of the planar conformations of aza-BODIQUs.

Photoluminescence in solution

The photoluminescence of complexes **1a**-**1e** in different solvents were investigated at room temperature. Their normalized emission spectra in CH_2Cl_2 at a concentration of 1 × 10^{-5} mol/L are illustrated in Fig. 3a. The emission band maxima and quantum yields are listed in Table 2. As we anticipated, connecting different electron-donating chromophors on the aza-BODIQU core directly can prominently help to achieve the aim that aza-BODIQU complexes **1a**-**1e** emit tunable emission varying from blue to red. Complex **1a** emits blue light in CH_2Cl_2 solution, and its stokes shift is quite small. Taking the feature into account, we can assign the observed emission to the $^1\pi$-π* state. Meanwhile, the emission of **1b**-**1d** are significantly red-shifted to green and yellow, due to the ICT process caused by the *N*-carbazolyl, 3,6-di-*tert*-butyl-*N*-carbazolyl and *N*-naphthalen-2-yl(phenyl)amino substituents with strong electron-donating ability. The dramatic bathochromic shifts of **1b**-**1d** in emission spectra are observed (Fig. S19, ESI†), owning to the intra-molecular electron push-pull effect. Whereas for **1e**, because of an aza-BODIQU core structure and two *N*-substituted phenothiazine chromophores with a twisted bowl-shaped configuration, thus, complex **1e** displays AIE effect and multi-stimuli responsive fluorescent properties.[13] All the complexes exhibit Φ_{PL} in the range of 0.24-0.78. Their Φ_{PL} in CH_2Cl_2 solution follow the trend of **1b** > **1c** > **1d** > **1e** > **1a**, in which complex **1b** exhibits the highest photoluminescence quantum yield (Φ_{PL} = 0.78) (Table 2). The minor solvatochromic effect and structured emission bands observed for **1a** indicate the $^1\pi$-π* dominated features of their emitting states (Fig. S19, ESI†). However, the emission bands of complexes **1c** and **1d** bathochromically shift in more polar solvents (*i.e.*, CH_2Cl_2 and CH_3CN) compared to those in solvents with lower polarity (*i.e.*, hexane and toluene). The drastic positive solvatochromic effect observed in complexes **1c** and **1d** should be attributed to the electron-donating groups (*N*-naphthalen-2-yl(phenyl)amino, and 3,6-di-*tert*-butyl-*N*-carbazolyl substituents), which enhances electron transfer from the symmetrical peripheral chromophores to the aza-BODIQU motif. To verify the involvement of ^{1}ICT character into the emitting states, the emission of the acid titration study of **1a**-**1d** has been investigated. Fig. 3c shows the emission spectra of **1c** with addition of *p*-TsOH. Upon addition of *p*-TsOH, the emission of **1c** at about 507 nm decreases, accompanied by the increase of a new relatively weak emission at about 627 nm, which exhibits a *ca.* 120 nm red-shift. This can be rationalized by the fact that protonation of the nitrogen atoms on the aza-BODIQU core increases the electron-withdrawing ability, which results in enhanced ^{1}ICT character and emission red-shifted. Similar phenomenon was observed for **1b** and **1d**, (Fig. S24, ESI†) whereas for **1a**, the emission at about 473 nm decreases, accompanied by the increase of a new relatively weak emission at about 428 nm, which exhibits a *ca.* 45 nm blue-shift. These ^{1}ICT features are also supported by the DFT calculation results.

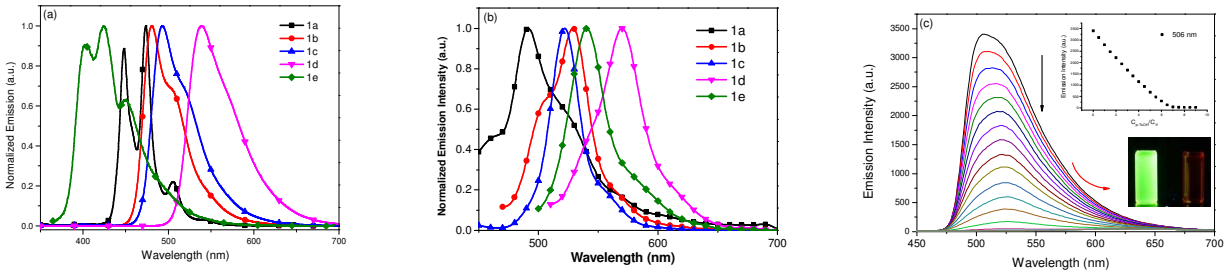

Fig. 3. Emission spectra of **1a**-**1e** in CH_2Cl_2 (1×10^{-5} M) (**a**); in solid state (**b**); (**c**) emission spectra of **1c** in CH_2Cl_2 with addition of *p*-TsOH /CH_3CN solution.

View Article Online
DOI: 10.1039/C4TC02955K

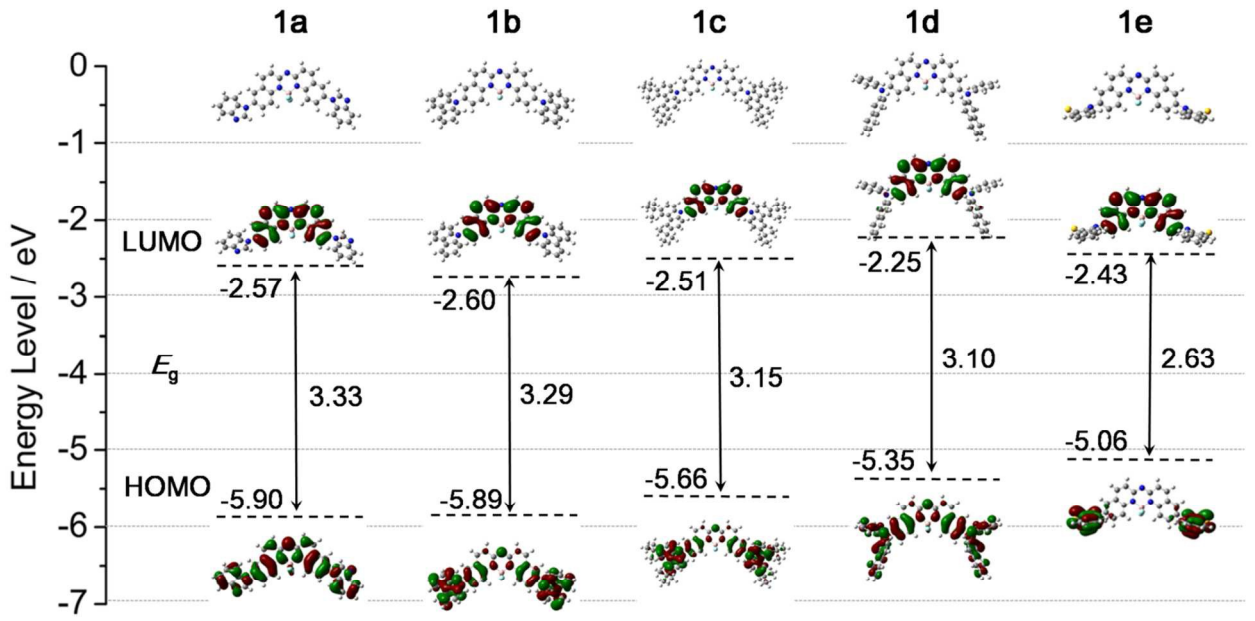

Fig 4. The optimized geometries and the molecular orbital surfaces of the HOMOs and LUMOs for aza-BODIQU **1a**-**1e** obtained at the B3LYP/6-31G* level.

Theoretical calculations

To understand the nature of the ground state and the low-lying excited states, quantum chemical calculations were performed for complexes **1a**-**1e**. The ground-state electron density distribution of the HOMO and LUMO are illustrated in Fig. 4. The HOMO-LUMO energy differences (energy band gaps, calculated E_g^{cal}) are presented in Table 3. The LUMOs of complexes **1a**-**1e** are almost delocalized on the aza-BODIQU cores. Due to the difference of dihedral angle (36° to 98°) between the *N*-substituents rings and the core structure, the π-electrons in the HOMO of **1a**-**1d** are delocalized over the entire molecule backbone, offering effective orbital interactions among the stacked π-systems. Meanwhile, the HOMOs of **1e** are localized on the *N*-aryl rings. Therefore, the HOMO→LUMO transition in **1a**-**1e** should be ascribed to a mixture of $^1\pi$-π^* mixed with different ^{1}ICT characters, which is consistent with their UV-vis absorption assignments. The results clearly demonstrate that strong electron-donating substituent, such as *N*-naphthalen-2-yl(phenyl)amino for **1d**, increases the energy level of HOMO more than that of LUMO. Thus the HOMO-LUMO gap decreases, causing a red-shift of the $^1\pi$-π^*/^{1}ICT absorption band. This not only follows the trend observed from the UV-vis absorption measurement but also explains the bathochromic shifts observed in the absorption, especially for **1d** bearing strong electron- donating *N*-naphthalen-2-yl(phenyl)amino substituents[19]. In addition, as is evident from Table 3, the trend of the predicted E_g^{cal} values is in consistent with the estimated E_g^{opt} from the ground-state absorption.

It is worthy to notice the optimized geometric structure of **1e**. The core structure of aza-BODIQU is planar, and the two *N*-substituted phenothiazine rings are nearly coplanar (the dihedral angle between two phenyl rings is 35°). However, the dihedral angles between the *N*-substituted phenothiazine rings and the core structure are 98°. This quite severe intramolecular torsion indicates that such a noncoplanar propeller-shaped structure will prevent the molecules from packing in a close π-π stacking mode. Thus, an AIE future is expected to observe from complex **1e**, and our previous work confirmed this.[13] In addition, as is evident from Table 3, the trend of the predicted E_g^{cal} values is consistent with the estimated E_g^{opt} from the ground-state absorption in Table 2.

pH sensor

Because of **1c** showing the most significant protonation effect among **1a**-**1d**, the pH sensor experiments of **1c** switching fluorescence from green to red were carried out. To certify the reversible transformation by protonation and deprotonation, the ^{1}H NMR spectra of protonation and deprotonation have been studied (Fig. 5). Addition of a drop of trifluoroacetic acid (TFA) into a chloroform solution of **1c** protonates its central *N* atom and generates **1c**-H^+ (Scheme 2). These protons shift downfield in the ^{1}H NMR spectra after protonation because of the transformation

Table 2. Optical properties of aza-BODIQUs **1a**-**1e** in CH_2Cl_2 solution and in solid-state.

Complex	λ_{max}^{abs} (nm) [a]			λ_{max}^{em} (nm) [b]		E_g^{opt} (eV) [c]		Φ_{PL} [d]
	CH_2Cl_2	Solid-state	ε_{max} (10^4 M^{-1} cm^{-1})	CH_2Cl_2	Solid-state	CH_2Cl_2	Solid-state	
1a	443	406	16.5	473	491	2.76	2.36	0.24
1b	457	415	11.4	483	529	2.59	2.24	0.78
1c	466	481	6.2	493	522	2.52	2.15	0.73

View Article Online
DOI: 10.1039/C4TC02955K

1d	505	465	7.5	540	570	2.32	1.97	0.51
1e	440	418	1.4	423	540	2.70	2.48	0.28

[a] Recorded in 1 × 10^{-5} M CH_2Cl_2 solution at r.t. [b] Recorded in 10^{-7} M CH_2Cl_2 solution of at r.t. [c] Optical band gaps determined from the absorption edge of the normalized absorption spectra. [d] Determined in CH_2Cl_2 using 9,10-diphenylanthracene (Φ_{PL} = 0.90 in cyclohexane) as standard at r.t.

Table 3. DFT calculation results of HOMO/LUMO energy levels.

Complex	LUMO (eV)	HOMO (eV)	E_g^{cal} (eV)[a]
1a	-2.57	-5.90	3.33
1b	-2.60	-5.89	3.29
1c	-2.51	-5.66	3.15
1d	-2.25	-5.35	3.10
1e	-2.43	-5.06	2.63

[a] Carried out at the B3LYP/6-31G* level of theory.

of **1c** change to an electron-deficient form **1c**-H^+. After adding excess triethylamine (TEA), the ^{1}H NMR spectra is fully recovered, suggesting that the reversible transformation between **1c** and **1c**-H^+. Based on the significant protonation effect, we envision that the fluorescence of **1c** could be switched by the solutions with different pH. Thus, we explored its application as a fluorescent pH sensor, using THF-buffer mixtures (1:9, *v/v*) with different pH as model compounds. As shown in Fig. 6a, **1c** in THF-buffer mixture (1:9, *v/v*) at pH 1 exhibits weak red fluorescence due to its transformation from **1c** to **1c**-H^+ under such acidic condition. At pH 2-4, the fluorescence of **1c** blue-shifted with the emission intensity increased, because the ratio of **1c**-H^+ decreases in the solutions. When pH increased from 5 to 10, the fluorescence intensity of **1c** at 507 nm was obviously enhanced. At pH = 10, the emission intensity become maximum. At pH 10-12, the emission intensity got a little weaker than the emission intensity at pH 10.

The pH sensor was also performed on the solid supports. Prepared filter paper of complex **1c** and buffer solutions with different pH were employed for experiments. As shown in Fig. 6b, the test paper shows faint red fluorescence under 365 nm UV light by addition of buffer solution at pH = 1. From pH 2 to 4, the emission blue-shift from yellow to green with intensity enhanced gradually. At pH > 5, the green emission was enhanced gradually until when pH=10 the emission got maximum, which is similar as the detections in the solutions. Evidently, the detections both in the solution and solid-state can also work well as a sensitive pH sensor. However, the detection in solid-state is much more rapid and convenient than that in the solution since the concentration in solid-state is much higher than in solution.

Moreover, the prepared test paper of **1c** can also used for acid and base vapours detection. The **1c** test paper shows strong green fluorescence under 365 nm UV light (Fig. 7). After exposing in hydrochloride (HCl) vapour, the fluorescence was tuned to red emission. Then fuming this test paper with triethylamine (TEA) for 5 min, the bright green fluorescence could be observed again. The switch between red and green can be repeated for more than three times. To further understand the protonation effect, DFT calculations of **1c** and **1c**-H^+ were performed. As shown in Fig. 8, the dihedral angles between the 3,6-di-*tert*-butyl-*N*-carbazolyl and the core structure in the optimized structure of **1c**-H^+ are both 43.0°, which are smaller than those in **1c** (52.3° and 53.2°). Thus, after protonation, its conformation becomes more planar and the C-N single bonds connecting the *N*-substituents and the core are also shorter (Table S5, ESI†). These results indicate better electronic communications in **1c**-H^+ with a high conjugation and hence a smaller energy band gap (Fig. S24, ESI†). Thus, the emission switches to red region. All these results demonstrate that complex **1c** is a fluorescence pH sensor with remarkable colour-changing.

Scheme 2. Reversible transformation between **1c** and **1c**-H^+ by repeated protonation and deprotonation.

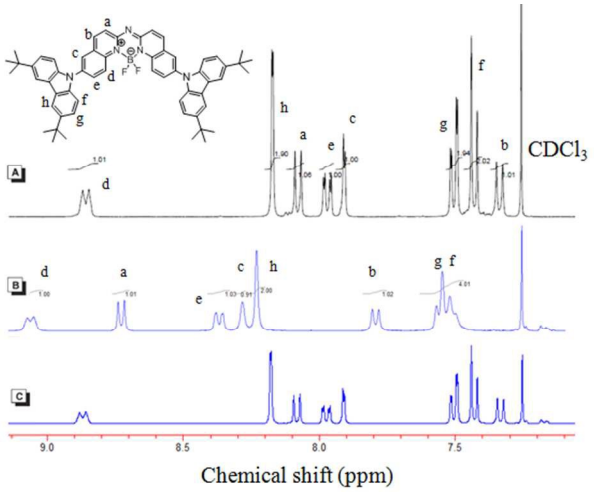

Fig. 5. ^{1}H NMR spectra of **1c** in $CDCl_3$ containing (A) 0 and (B) 10 μL TFA (C) adding 50 μL triethylamine (TEA) into (B).

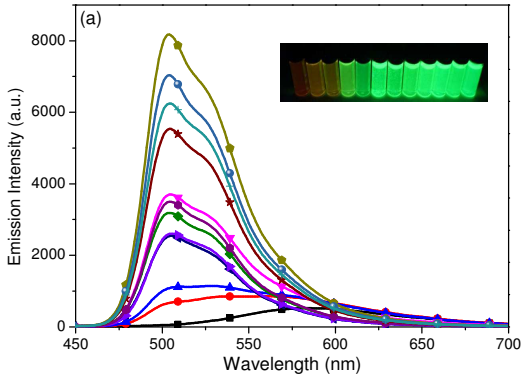

View Article Online
DOI: 10.1039/C4TC02955K

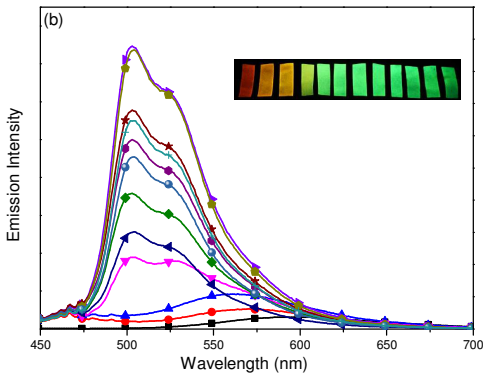

Fig. 6. Effect of pH on (a) PL spectra of **1c** in THF-buffer mixtures (1/9, v/v) and (b) deposited on filter paper. Insets in (a and b): fluorescent photos at pH 1 (left) to 12 (right) taken under 365 nm UV irradiation.

Experimental section

Synthesis

All solvents and reagents employed were purchased from Aldrich or Sinopharm Chemical Regent Co. Ltd. and used as received unless otherwise stated. Tetrahydrofuran (THF) and toluene were distilled under N_2 over sodium benzophenone ketyl. Tetra-*n*-butylammonium perchlorate (TBAP) and ferrocene were purified by recrystallization twice from ethanol. Silica gel (300-400 mesh) used for chromatography was purchased from Sinopharm Chemical Reagent Co. Ltd. Buffer solutions with pH 1 to 12 were purchased from Sigma-Aldrich.

Instruments

^{1}H NMR and ^{13}C NMR spectra were recorded on a Bruker 300 MHz or 400 MHz spectrometer using DMSO-d_6 or $CDCl_3$ as the solvent. Chemical shifts were referred to the internal standard tetramethylsilane (TMS). ^{19}F NMR spectra were recorded at room temperature with $CFCl_3$ as internal standard at 376 MHz. Melting points (m.p.) were taken on an X-4 microscope electrothermal apparatus (Taike China). The elemental analyses were performed with a Vario El III elemental analyzer. Mass spectra were obtained on a VG12-250 mass spectrometer and an Agilent 1100 mass spectrometer. UV-Vis spectra were recorded using an HP-8453 UV/Vis/near-IR spectrophotometer (Agilent) with a 1 cm quartz cell. Photoluminescence spectra were carried out on a F-4600 FL Spectrophotometer (Hitachi). Photoluminescence quantum yields were carried out on a F-4600 FL Spectrophotometer (Hitachi). Powder X-ray diffraction (XRD) patterns of the samples were collected on a Bruker D8 Advance powder diffractometer. Electrochemical experiments were carried out using a CHI 660C electrochemistry workstation (CHI-USA). A standard one-compartment three-electrode cell was used with a Pt electrode as the working electrode, a Pt wire as the counter electrode and an $Ag/AgNO_3$ electrode (Ag in 0.1 M $AgNO_3$ solution) as the reference electrode. TBAP (0.1 M) was used as the supporting electrolyte. The scan rate was 100 mV S^{-1}. Differential scanning calorimetry (DSC) was conducted on a DSC instruments (NETZSCH DSC 204).

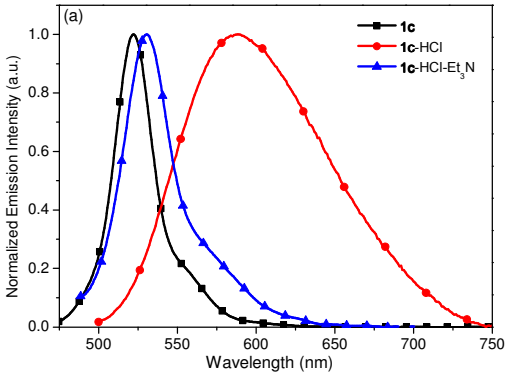

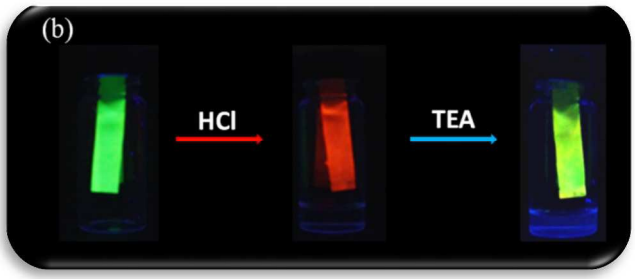

Fig. 7. (a) Emission spectra of initial, HCl fumed and TEA fumed test paper of **1c**; (b) **1c** paper samples (left to right: blank, HCl vapor fumed sample, TEA vapor fumed sample after fumed by HCl vapor) taken under UV light.

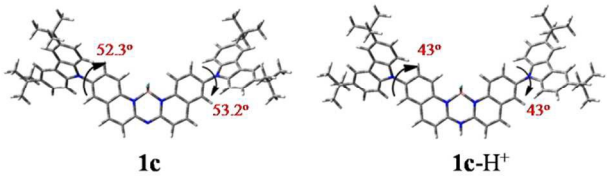

Fig. 8. The dihedral angles of the rings between nitrogen heterocyclic rings and cores according to the ground-state optimized structure of **1c** and 1c-H^+ in gas state.

X-ray diffraction crystallography

Crystals **1b, 1c and 1e** were grown by the slow evaporation of their solutions in the mixture solvent of ethyl acetate and petroleumether at room temperature. All diffraction data were collected on a Rigaku Saturn diffractometer with a CCD area detector. All calculations were performed by using SHELXL97 and the crystallographic software packages. CCDC 885792 (**1b**), CCDC 1021584 (**1c**) and CCDC 996071 (**1e**) contain the supplementary crystallographic data for this paper.

DFT calculations

All the calculations were carried out using Gaussian 09 program package. The geometries of complexes **1a-1e** were fully optimized at B3LYP/6-31G* level. Harmonic vibrational frequencies were calculated at the same level to check whether the obtained structure is a minimum. The frontier molecular orbitals were calculated for each of the compounds. In this work, all the calculations were performed in vacuum without considering the solvent.

View Article Online
DOI: 10.1039/C4TC02955K

Synthesis of difluoro-boron complex of bis(6-bromoquinolin-2-yl)amine (BrQNBF)

Compound **2** (6-bromoquinoline *N*-oxide), **3** (2,6-dibromoquinoline), **4** (6-bromoquinolin-2-amine), **5** (bis(6-bromoquinolin-2-yl)amine) and **BrQNBF** (difluoro-boron complex of bis(6-bromoquinolin-2-yl)amine) were synthesized according to the reference.[12]

General procedure for synthesis of 1a-1e

To a round bottom flask was charged **BrQNBF** (237 mg, 0.5 mmol), arylamines(1.1 mmol), *t*-BuONa (120 mg, 1.2 mmol), $Pd(OAc)_2$ (6 mg, 0.025 mmol, 5% mol), *t*-Bu_3P (0.05 mmol) and 3 mL toluene[14]. The reaction mixture was refluxed under N_2 for 12 h. After cooling to r.t., it was diluted with brine (20 mL) and extract with CH_2Cl_2 (3 × 30 mL). The organic layer was then dried with Na_2SO_4 and the solvent was removed under reduced pressure. The product was purified by silica gel column chromatography (CH_2Cl_2 / hexane).

Difluoro-boron complex of bis(6-(*N*-benzoimidazolyl) quinolin-2-yl) amine (1a)

128 mg of yellow solid was obtained, yield 54%, m.p. = 264-266 °C. ^{1}H NMR (400 MHz, $CDCl_3$) δ 8.48 (d, J = 9.6 Hz, 4H), 7.93 (d, J = 9.2 Hz, 4H), 7.84 (d, J = 2 Hz, 4H), 7.80 (d, J = 2.4 Hz, 2H), 7.78 (d, J = 2.4 Hz, 2H), 7.21 (d, J = 8.8Hz, 4H). ^{19}F NMR (376 MHz, $CDCl_3$) δ -126.25 (q, $J_{B,F}$ = 78.0 Hz).

Difluoro-boron complex of bis(6-(*N*-carbazolyl) quinolin-2-yl)amine (1b)

221 mg of yellow solid was obtained, yield 69%, m.p. > 300 °C. ^{1}H NMR (400 MHz, $CDCl_3$) δ 8.91-8.88 (m, 2H), 8.18 (d, J = 7.7 Hz, 4H), 8.09 (d, J = 9.1 Hz, 2H), 7.97 (dd, J = 9.2, 2.4 Hz, 2H), 7.92 (d, J = 2.3 Hz, 2H), 7.52-7.40 (m, 8H), 7.40-7.29 (m, 6H). ^{13}C NMR (100 MHz, $CDCl_3$) δ 154.35, 140.75, 140.29, 137.21, 134.75, 130.12, 126.22, 125.91, 125.68, 123.91, 123.71, 123.60, 120.50, 120.43, 109.55. ^{19}F NMR (376 MHz, $CDCl_3$) δ -126.10 (q, $J_{B,F}$ = 73.4 Hz). Elemental analysis calcd. (%) for $C_{42}H_{26}BF_2N_5$: C, 77.67; H, 4.03; N, 10.78 , found C 77.49; H, 4.11; N, 10.85. Crystal data for **1b** ($C_{48}H_{38}BF_2N_5O_2$): Mr = 765.64, triclinic, space group P1(2), a = 9.0720(18) Å, b = 15.181(3) Å, c = 16.186(3) Å, α = 65.63(3)°, β = 86.22(3)°, γ = 77.79(3)°, V = 1984.05(70) Å^3, Z = 2, ρ_{calcd} = 1.281 g/cm^3, T = 293(2) K, Crystal size 0.11 × 0.26 × 0.28 mm^3, R_1 = 0.0767, wR_2 = 0.1565, [I > 2sigma(I)].

Difluoro-boron complex of bis(6-(3,6-di-tert-butyl-*N*-carbazolyl) quinolin-2-yl) amine (1c)

196 mg of yellow solid was obtained, yield 73%, m.p. = 250-251 °C. ^{1}H NMR (400 MHz, $CDCl_3$) δ 8.87 (d, J = 9.2 Hz, 2H), 8.18 (d, J = 1.6 Hz, 4H), 8.07 (d, J = 9.1 Hz, 2H), 7.97 (dd, J = 9.3, 2.4 Hz, 2H), 7.90 (d, J = 2.4 Hz, 2H), 7.50 (dd, J = 8.7, 1.9 Hz, 4H), 7.43 (d, J = 8.6 Hz, 4H), 7.33 (d, J = 9.1 Hz, 2H). ^{13}C NMR (100 MHz, $CDCl_3$) δ 154.27, 143.46, 140.29, 139.10, 136.93, 135.29, 129.85, 125.96, 125.11, 123.77, 123.53, 116.48, 109.01, 34.83, 32.05. ^{19}F NMR (376 MHz, $CDCl_3$) δ -126.27 (q, $J_{B,F}$ = 73.4 Hz). Elemental analysis calcd. (%) for $C_{58}H_{58}BF_2N_5$: C, 79.71; H, 6.69; N, 8.01, found C 79.59; H, 6.76; N, 8.15. Crystal data for **1c** ($C_{58}H_{58}BF_2N_5$): Mr = 873.90, monoclinic, space group $P2_1/c$, a = 22.4457(17) Å, b = 11.3035(7) Å, c = 20.0181(14) Å, α = 90°, β = 92.623(5)°, γ = 90°, V = 5073.6(6) Å^3, Z = 4, ρ_{calcd} = 1.144 g/cm^3, T = 296 K, Crystal size 0.30 × 0.15 × 0.10 mm^3, R_1 = 0.1316, wR_2 = 0.2674, [I > 2sigma(I)].

Difluoro-boron complex of bis(6-(*N*-naphthalen-2-yl-phenylamino) quinolin-2-yl) amine (1d)

145 mg of yellow solid was obtained, yield 64%, m.p. = 283-284 °C. ^{1}H NMR (400 MHz, $CDCl_3$) δ 8.47 (d, J = 9.4 Hz, 2H), 7.76 (dd, J = 17.7, 8.6 Hz, 6H), 7.62 (d, J = 7.7 Hz, 2H), 7.58-7.48 (m, 4H), 7.46-7.36 (m, 4H), 7.31 (dd, J = 8.0, 5.4 Hz, 8H), 7.19 (d, J = 7.7 Hz, 4H), 7.15-7.08 (m, 4H). ^{13}C NMR (100 MHz, $CDCl_3$) δ 153.14, 147.22, 144.84, 139.67, 134.42, 134.20, 130.42, 129.60, 129.31, 127.73, 127.10, 126.50, 125.98, 124.84, 124.49, 123.75, 123.04, 122.80, 121.05, 120.47. ^{19}F NMR (376 MHz, $CDCl_3$) δ -127.18 (q, $J_{B,F}$ = 73.6 Hz). Elemental analysis calcd. (%) for $C_{50}H_{34}BF_2N_5$: C, 79.68; H, 4.55; N, 9.29, found C 79.59; H, 4.51; N, 9.25.

Difluoro-boron complex of bis(6-(*N*-phenothiazinyl) quinolin-2-yl) amine (1e)

121 mg of yellow solid was obtained, yield 65%, m.p. > 300 °C. ^{1}H NMR (400 MHz, $CDCl_3$) δ 8.82 (d, J = 9.1 Hz, 2H), 8.04 (d, J = 9.1 Hz, 2H), 7.81-7.68 (m, 4H), 7.29 (s, 2H), 7.12 (dd, J = 7.3, 1.6 Hz, 4H), 6.99-6.82 (m, 8H), 6.42 (d, J = 7.7 Hz, 4H). ^{13}C NMR (100 MHz, $CDCl_3$) δ 143.75, 140.33, 138.53, 132.59, 127.12, 126.69, 124.20, 123.30, 122.23, 117.53. ^{19}F NMR (376 MHz, $CDCl_3$) δ -126.26 (q, $J_{B,F}$ = 73.3 Hz). Elemental analysis calcd. (%) for $C_{58}H_{34}BF_2N_5$: C, 81.98; H, 4.03; N, 8.24, found C 82.09; H, 4.11; N, 8.15. Crystal data for **1e** ($C_{42}H_{26}BF_2N_5S_2$): Mr = 713.61, triclinic, space group P-1, a = 8.2448(13) Å, b = 13.187(2) Å, c = 19.061(3) Å, α = 100.053(14)°, β = 95.703(13)°, γ = 95.546(12)°, V = 2016.7(6) Å^3, Z = 2, ρ_{calcd} = 1.175 g/cm^3, T = 293(2) K, R_1 = 0.0952, wR_2 = 0.2014, [I > 2sigma(I)].

Conclusions

A series of new aza-boron-diquinomethene complexes (**1a**-**1e**) bearing different *N*-arylamines has been designed and synthesized. Their thermal stabilities and photophysical properties were investigated systematically. All these complexes show robust thermal stability with high melt transitions temperatures (> 250 °C). All complexes exhibit strong $^1\pi$-π* transfer mixed with varying degrees of ^{1}ICT characters and intense blue to red $^1\pi$-π*/^{1}ICT emission with different photoluminescence quantum yields (0.24-0.78). Their photoluminescence quantum yields follow the trend of **1b** > **1c** > **1d** > **1e** > **1a**. These results indicate that the direct connection of *N*-arylamino groups onto the core structure is a succeed strategy which would be useful for rational design of new aza-BODIQU molecules. In addition, the application of **1c** for pH sensor based on its remarkable colour-changing property has been investigated, which can be used in both the solution and solid states as well as acid and base vapours. All these results indicate that these complexes exhibit the robust thermal stability, tunable photophysical properties, relatively high photoluminescence quantum yields and protonation effect, make these complexes potential candidates for applications in pH sensor, bioimaging

View Article Online
DOI: 10.1039/C4TC02955K

probe, organic light-emitting materials and data security protection.

Acknowledgment

The authors greatly acknowledge the financial support in part by Postgraduate Innovation Fund of Jiangsu Province (2013, CXZZ13_0459; 2014, KYLX_0774), Natural Science Foundation of the Jiangsu Higher Education Institutions of China (13KJB150018), Natural Science Foundation of Jiangsu Province (BK20130926).

Notes and references

a Department of Applied Chemistry, College of Sciences, Nanjing Tech University, Nanjing 211816, P. R. China. E-mail: zhuhj@njtech.edu.cn; rui.liu@njtech.edu.cn.

b Department of Chemistry, Fudan University, Shanghai 200433, P. R. China.

† Electronic Supplementary Information (ESI) available: structural characterization data, crystal stacking spectra, calculation and photophysical studies. CCDC 885792, 1021584 and CCDC 996071. For ESI and crystallographic data in CIF or other electronic format see DOI: 10.1039/c000000x.

1 (a) A. Loudet and K. Burgess, *Chem. Rev.,* 2007, **107**, 4891; (b) N. Boens, V. Leen and W. Dehaen, *Chem. Soc. Rev.,* 2012, **41**, 1130; (c) G. Ulrich, R. Ziessel and A. Harriman, *Angew. Chem. Int. Ed.*, **2008**, 47, 1184.

2 (a) S. Atilgan, Z. Ekmekci, A. L. Dogan, D. Guc and E. U. Akkaya, *Chem. Commun.*, 2006, **42**, 4398. (b) S. Erbas, A. Gorgulu, M. Kocakusakogullari and E. U. Akkaya, *Chem. Commun.*, 2009, **33**, 4956. (c) S. Ozlem and E. U. Akkaya, *J. Am. Chem. Soc.*, 2009, **131**, 48.

3 R. Ziessel, G. Ulrich and A. Harriman, *New J. Chem.*, 2007, **31**, 496.

4 (a) P. A. Bouit, K. Kamada, P. Feneyrou, G. Berginc, L. Toupet, O. Maury and C. Andraud, *Adv. Mater.*, 2009, **21**, 1151. (b) D. Zhang, Y. Wang, Y. Xiao, S. Qian and X. Qian, *Tetrahedron*, 2009, **65**, 8099.

5 (a) S. Hattori, K. Ohkubo, Y. Uran, H. Sunahara, T. Nagano, Y. Wada, N. V. Tkachenko, H. Lemmetyinen, S. Fukuzumi, *J. Phys. Chem. B,* 2005, **109**, 15368. (b) S. Erten-Ela, D. Yilmaz, B. Icli, Y. Dede, S. Icli and E. U. Akkaya, *Org. Lett.*, 2008, **10**, 3299. (c) T. Rousseau, A. Cravino, T. Bura, G. Ulrich, R. Ziessel and J. Roncali, *Chem. Commun.*, 2009, **13**, 1673. (d) T. Rousseau, A. Cravino, T. Bura, G. Ulrich, R. Ziessel, *J. Mater. Chem.*, 2009, **19**, 2298. (e) J. C. Forgie, P. J. Skabara, I. Stibor, F. Vilela and Z. Vobecka, *Chem. Mater.*, 2009, **21**, 1784. (f) S. Kolemen, Y. Cakmak, S. Erten-Ela, Y. Altay, J. Brendel, M. Thelakkat and E. U. Akkaya, *Org. Lett.*, 2010, **12**, 3812. (g) C. Y. Lee and J. T. Hupp, *Langmuir*, 2010, **26**, 3760.

6. (a) D. Frath, J. Massue, G. Ulrich and R. Ziessel, *Angew. Chem. Int. Ed.* 2014, **53**, 2290; (b)M. Hesari, J. S. Lu, S. N. Wang and Z. F. Ding, *Chem. Commun.*, 2015, DOI: 10.1039/C4CC08671F.

7 (a) A. Poirel, A. D. Nicola and R. Ziessel, *Org. Lett.*, 2012, **14**, 5696; (b) L. Gao, N. Deligonul and T. G. Gray, *Inorg. Chem.*, 2012, **51**, 7682; (c) Y. Kubota, T. Tsuzuki, K. Funabiki, M. Ebihara and M. Matsui, *Org. Lett.*, 2010, **12**, 4010; (d) H. J. Li, W. F. Fu, L. Li, X. Gan, W. H. Mu, W. Q. Chen, *et al*, *Org. Lett.*, 2010, **12**, 2924; (e) S. Chibani, B. L. Guennic, B. Charaf-Eddin, O. Maury, C. Andraud and D. Jacquemin, *J. Chem. Theory Comput.*, 2012, **8**, 3303; (f) H. Sasabe and J. Kido, *Chem. Mater.*, 2011, **23**, 621.

8 (a) S. P. Singh and T. Gayathri, *Eur. J. Org. Chem.*, 2014, **22**, 4689; (b) S. Kolemen, Y. Cakmak, S. Erten-Ela, Y. Altay, J. Brendel, M. Thelakkat and E. U. Akkaya, *Org. Lett.* 2010, 12, 3812; (c) Y. Kubo, K. Watanabe, R. Nishiyabu, R. Hata, A. Murakami, T. Shoda and H. Ota, *Org. Lett.* 2011, **13**, 4574.

9 (a) J. Murtagh, D. O. Frimannsson and D. F. O'Shea, *Org. Lett.*, 2009, **11**, 5386; (b) J. Shao, H. Guo, S. Ji and J. Zhao, *Biosens. Bioelectron.*, 2011, **26**, 3012; (c) S. Hoogendoorn, A. E. M. Blom, L. I. Willems, G. A. van der Marel and H. S. Overkleeft, *Org. Lett.*, 2011, **13**, 5656.

10 (a) T. W. Kwon, M. M. Alam and S. A. Jenekhe. *Chem. Mater.*, 2004, **23**, 4657. (b) C. J. Tonzola, M. M. Alam, W. Kaminsky and S. A. Jenekhe. *J. Am. Chem. Soc.*, 2003, **125**, 13548.

11 M. E. Kondakova, J. C. Deaton, T. D. Pawlik, D. J. Giesen, D. Y. Kondakov and R. H. Young, et al. *J. Appl. Phys.*, 2010, **107**, 014515.

12 D. F. Wang, R. Liu, C. Chen, S. F. Wang, J. Chang, C. H. Wu, H. J. Zhu and E. R. Waclawik. *Dyes Pigments*, 2013, **99**, 240.

13 X. L. Zhu, R. Liu, Y. H. Li, H. Huang, Q. Wang, D. F. Wang, X. Zhu, S. S. Liu and H. J. Zhu. *Chem. Commun.*, 2014, **50**, 12951.

14 (a) M. Su, N. Hoshiya and S. L. Buchwald. *Org. Lett.*, 2014, **16**, 832. (b) M. Su and S. L. Buchwald. *Angew. Chem. Int. Ed.*, 2012, **51**, 4710.

15 (a) G. M. Sheldrick. Germany: University of Göttingen, 1997. (b) Siemens. SHELXTL. Version 5.06. Madison, Wisconsin, USA: Siemens Analytical X-ray Instruments Inc; 1996.

16 (a) D. B. Axel. J. Chem. Phys., 1993, **7**, 5648. (b) C. Lee, W. Yang, and R. G. Parr. *Phys. Rev. B*, 1988, **37**, 785.

17 (a) T. Clark, J. Chandrasekhar, G. W. Spitznagel and P. R. Schleyer. *J. Comput. Chem.*, 1983, **4**, 294. (b) M. M. Francl, W. J. Pietro, W. J. Hehre, J. S. Binkley, M. S. Gordon, D. J. DeFrees and J. A. Pople. *J. Chem. Phys.*, 1982, **77**, 3654. (c) P. M. Y. Gill, B. G. Johnson, J. A. Pople and M. J. Frisch. Chem. Phys. Lett., 1992, **197**, 499. (d) P. C. Hariharan and J. A. Pople. Theoretica Chimica Acta, 1973, **28**, 213. (e) R. Krishnan, J. S. Binkley, R. Seeger and J. A. Pople. *J. Chem. Phys.*, 1980, **72**, 650.

18 M. J. Frisch, G. W. Trucks, H. B. Schlegel, G. E. Scuseria, M. A. Robb and J. R. Cheeseman, *et al*. Gaussian 09, revision B. 01. Wallingford CT: Gaussian, Inc; 2010.

19 J. Bañuelos, F. L. Arbeloa, V. Martinez, M. Liras, A. Costela and I. G. Moreno, et al. *Phys. Chem. Chem. Phys.*, 2011, **13**, 3437.

20 M. Couturier and T. Le. *Org. Process Res. Dev.*, 2006, **10**, 534.

21 C. Q. Zhang, S. B. Jin, K. N. Yang, X. D. Xue, Z. P. Li, Y. G. Jiang, W. Q. Chen, L. R. Dai, G. Z. Zou and X. J. Liang. *ACS Appl. Mater. Inter.*, 2014, **6**, 8971.

View Article Online
DOI: 10.1039/C4TC02955K

A series of new aza-boron-diquinomethene complexes (**1a-1e**) with tunable photophysical properties has been designed and synthesized.